Langmuir

Article

Study on the surface energy of graphene by contact angle measurement

Andrew Kozbial, Zhiting Li, Caitlyn Conaway, Rebecca McGinley, Shonali Dhingra, Vahid Vahdat, Feng Zhou, Brian D'Urso, Haitao Liu, and Lei Li

Langmuir, **Just Accepted Manuscript** • DOI: 10.1021/la5018328 • Publication Date (Web): 01 Jul 2014

Study on the surface energy of graphene by contact angle measurements

Andrew Kozbial [a‡], Zhiting Li [b‡], Caitlyn Conaway [a], Rebecca McGinley [a], Shonali Dhingra [c], Vahid Vahdat [a], Feng Zhou [b], Brian D'Urso [c], Haitao Liu [b*], and Lei Li [a,d,*]

[a] Department of Chemical & Petroleum Engineering, Swanson School of Engineering, University of Pittsburgh, Pittsburgh, PA, USA

[b] Department of Chemistry, University of Pittsburgh, Pittsburgh, PA 15260, USA

[c] Department of Physics and Astronomy, University of Pittsburgh, Pittsburgh, PA 15260, USA

[d] Department of Mechanical Engineering & Materials Science, Swanson School of Engineering, University of Pittsburgh, Pittsburgh, PA, USA

[‡]: These authors contribute equally to this work

*: Corresponding author. Email: lel55@pitt.edu (L.L.); hliu@pitt.edu (H. L.)

Abstract

Due to the atomic thinness of graphene, its integration into a device will always involve its interaction with at least one supporting substrate, making the surface energy of graphene critical to its real-life applications. In the current paper, the contact angle of graphene synthesized by chemical vapor deposition (CVD) was monitored temporally after synthesis using water, diiodomethane, ethylene glycol, and glycerol. The surface energy was then calculated based on the contact angle data by Fowkes, Owens-Wendt (extended Fowkes), and Neumann models. The surface energy of fresh CVD graphene grown on a copper substrate (G/Cu) immediately after synthesis was determined to be 62.2±3.1 mJ/m^2 (Fowkes), 53.0±4.3 mJ/m^2 (Owens-Wendt) and 63.8±2.0 mJ/m^2 (Neumann), which decreased to 45.6±3.9 mJ/m^2, 37.5±2.3 mJ/m^2 and 57.4±2.1 mJ/m^2, respectively, after 24 hours of air exposure. The ellipsometry characterization indicates that the surface energy of G/Cu is affected by airborne hydrocarbon contamination. G/Cu exhibits the highest surface energy immediately after synthesis and the surface energy decreases after

airborne contamination occurs. The root-cause of intrinsically mild polarity of G/Cu surface is discussed.

1. Introduction

Graphene exhibits interesting electrical, optical, mechanical, and chemical properties which make it a candidate material in many important applications, including transistors, sensors, transparent conductors, and clean energy devices [1–6]. Due to its atomic thinness, graphene must be bound to at least one substrate for most applications. As a result, the adhesion between graphene and other materials is critical for the device fabrication [7–10]. Since the adhesion is largely dependent on the surface energy, it is important to determine the surface energy of graphene. Moreover, the surface energy is also critical to the adsorption process, which has been shown to affect the properties of graphene [11].

Although several research groups have conducted contact angle measurements on graphene, analysis was seldom extended to surface energy calculations. Shin *et al.* conducted water contact angle (WCA) measurements on epitaxial graphene grown on SiC and reported WCA on the graphene as 92° [10]. Kim *et al*. reported the WCA of CVD-grown graphene transferred to SiO_2 as 90.4° and 93.8° for Ni-grown and Cu-grown graphene, respectively [12]. Moreover, Rafiee *et al.* reported the WCA of G/Cu to be 86° [4]. These results on single- and multi-layer graphene are generally consistent with WCA values on graphite and highly oriented pyrolytic graphite (HOPG) [7,10,13–15]. More recently, Li *et al*. showed that WCA of CVD-grown G/Cu tested within 10 seconds after synthesis was 44° and increased to 80° after 1 day exposure in ambient air. The increase of hydrophobicity was attributed to the adsorption of airborne hydrocarbon contaminants onto the initially clean surface and this conclusion was supported by Attenuated Total Reflection Fourier Transform Infrared Spectroscopy (ATR-FTIR) and X-ray Photoelectron Spectroscopy (XPS) experiments [15]. A parallel study by Gomez-Herrero *et al.* also concluded that graphite is

contaminated by hydrocarbons using Kelvin probe force microscopy and mass spectrometry techniques [16].

Although WCA data provides valuable information on the wettability of a surface, many other surface properties are related to the surface free energy. Surface energy (γ) is a key parameter characterizing the solid surface and its interaction with other materials. It has been well recognized that this parameter is closely related to not only wettability, but also many other important properties at the surface interface, *e.g.*, adhesion and friction [17,18]. Therefore, measuring the surface energy of graphene is important for both fundamental study and applications of graphene [19]. Although numerous studies on the electrical and optical properties of graphene have been reported in literature, to date only a few published reports have characterized the surface free energy of graphene. Wang *et al.* produced graphene sheets through chemical exfoliation of natural graphite flake and hydrazine conversion and then assembled graphene sheets into a film. They determined the surface energy of the graphene film by contact angle testing using Neumann model and concluded that the surface energy of the graphene film and graphite was 46.7 mJ/m^2 and 54.8 mJ/m^2, respectively [7]. Based on the exfoliation experiments of graphite in various solvents, Coleman *et al.* reported surface energy values of 65-90 mJ/m^2 for graphene/graphite [20,21].

Contact angle testing [22,23], schematically shown in Figure 1, is experimentally simpler than most other characterization methods. Usually, several testing liquids with different polar and dispersive components are used for testing [24]. Table 1 lists the polar and dispersive surface energy components of the four test liquids used in this study: water (W), diiodomethane (DIM), ethylene glycol (EG), and glycerol (G) [9]. Several models have been proposed to translate contact angle data to surface energy [17,18,25] and the validity of these models is still a matter of debate. In the current study, Fowkes model [25], Owens-Wendt (extended Fowkes) model [17], and Neumann model

[18] were used for determining the surface energy from contact angle data. The analysis based on Fowkes and Owen-Wendt models indicated that the fresh graphene/copper surface has significant polar components, which provide additional insights into the nature of the intrinsic mildly hydrophilic of the substrate. Additionally, since the copper substrate used to support graphene is rough, AFM and WCA experiments were conducted to elucidate the potential effect of substrate roughness on the observed contact angle and calculated surface energy of supported graphene.

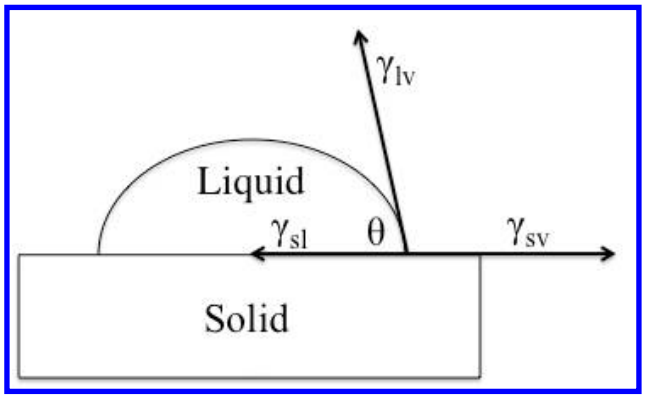

Figure 1. Schematic depicting the interfaces of a liquid droplet on a solid surface [26].

Table 1. Polar and dispersive surface energy components of the test liquids.

	γ_l (mJ/m^2)	γ_l^p (mJ/m^2)	γ_l^d (mJ/m^2)
Water (W)	72.8	51.0	21.8
Diiodomethane (DIM)	50.8	0.0	50.8
Ethylene glycol (EG)	48.0	19.0	29.0
Glycerol (G)	64.0	30.0	34.0

2. Experiments

2.1. Materials

DI water was produced from a Millipore Academic A10 system with total organic carbon below 40 ppb. Diiodomethane (99%), ethylene glycol (99.8%), and glycerol (99%) were purchased from Sigma-Aldrich and used as received. Copper foil (99.8%, 25 μm thick) was purchased from Alfa Aesar and used as received. HOPG (SPI-2 grade; 20 × 20 × 1 mm) was purchased from SPI and used as received. The HOPG sample was carefully exfoliated with adhesive tape to expose a fresh surface.

2.2. Synthesis of CVD graphene

Four copper foil samples (Alfa Aesar, 99.8%, 25 μm thick) each ~ 4 cm^2 in size were placed at the center of a 1-inch-diameter fused quartz tube. The tube was evacuated and heated to 1000°C under a 2.0 standard cubic centimeter per minute (sccm) H_2 gas flow at a pressure of 100-110 mTorr for 30 min, followed by CH_4 (carbon source) gas flow of 20 sccm at 1000°C for another 30 min at a total pressure of 500 mTorr. Then the copper foil was cooled to room temperature under H_2 and CH_4 gas flow and taken out from the tube furnace. One G/Cu sample was tested immediately and referenced to as "fresh" surface. This sample was exposed to air only during transfer from the CVD chamber to the contact angle instrument (~30 seconds until first contact angle test). The remaining samples were placed in a fume hood to ensure a consistent airborne hydrocarbon contamination level. One liquid was used to test the same batch of samples and testing using different liquids (water, diiodomethane, ethylene glycol, glycerol) was conducted on different batches of samples.

2.3. Characterization

2.3.1. Raman Spectroscopy. Room temperature micro-Raman spectra were taken using a home built instrument using a laser excitation of 532 nm (2.33 eV). The instrument configuration has

been described elsewhere [27,28]. The integration time was 60 seconds and a low incident power less than 1 mW was used to avoid unwanted heating effects from the laser.

2.3.2. Atomic force microscopy. AFM imaging was performed in tapping mode on a Veeco Dimension V instrument using an NSC15 Al-backside (MikroMasch; 40 N/m; 325 kHz) cantilever probe.

2.3.3. Contact angle measurement. Contact angle measurements were conducted with a VCA Optima XE at ambient temperature (22-25°C) and relative humidity (20-40%). A separate testing syringe was dedicated for each test liquid to avoid cross-contamination. A liquid droplet of 2 μL was formed at the end of the syringe and carefully deposited onto the sample surface. The syringe was withdrawn and the image of static contact angle was taken within 3 seconds of liquid deposition by a charge coupled device (CCD) camera. The contact angle was calculated by vendor-supplied software. The reported contact angle values are based on 5-8 repeats.

2.3.4. Spectroscopic ellipsometry. Ellipsometry measurements were performed with a J.A. Woollam Co. Alpha-SE spectroscopic ellipsometer at a wavelength range of 380 nm to 900 nm and 70° incident angle. Within 5 minutes of being removed from the CVD-chamber, freshly synthesized G/Cu was placed on the ellipsometric sample stage and *in situ* data was collected without moving the sample at 10-second intervals with an acquisition time of 10 seconds. Ellipsometry measures the change in Ψ and Δ of polarized light after interacting with a surface. Here Ψ represents the shift in amplitude and Δ represents the shift in phase of the polarized light [29–32]. Previous studies have showed that the change in phase shift (δΔ) is proportional to the film thickness [32,33]. The organic contamination on SiO_2 has been characterized with ellipsometry and an increase of Δ with exposure time to organic contaminants was reported [29]. In the current study,

ellipsometry characterization was conducted on G/Cu samples with respect to the aging time in ambient air to monitor the possible airborne hydrocarbon contamination. Since Δ is most sensitive to thickness changes at low wavelength [34], we monitored Δ at 501 nm and compared initial Δ on fresh G/Cu to the Δ value obtained on the aged surface. The difference $[\Delta_{fresh} - \Delta_{aged}(time)]_{wavelength = 501nm}$ was taken as δΔ and plotted against the time exposed to ambient air.

3. Surface energy models

Several methods based on surface energy theory have been developed and further details can be found in several literature reviews [35–38]. In the current paper, three models – Fowkes model [25], Owens-Wendt (extended Fowkes) model [17], and Neumann model [18] – were used to calculate the surface energy of graphene from contact angle data. Fowkes model and Owen-Wendt model allow for dissociation of the total surface energy into polar and non-polar (dispersive) components which provides further insight to surface properties [17,25]. We note that the calculated surface energy will depend on the model used, even if the same contact angle data was used. The objective of this study was not to determine the validity of models, which has been a matter of debate for decades. Instead, we want to utilize commonly accepted surface energy models to estimate the surface energy of graphene samples and understand the key factors controlling the surface energy.

3.1. Neumann model

Neumann's equation of state theory describes the contact angle (θ) of a liquid on a solid surface as [7,18,39,40]:

$$\cos\theta = -1 + 2\sqrt{\frac{\gamma_s}{\gamma_l}}e^{-\beta(\gamma_s - \gamma_l)^2} \qquad (1)$$

where γ_s is the solid free surface energy, γ_l is the liquid free surface energy, θ is the contact angle, and β is a parameter related to the solid surface. Rearrangement of (1) results in:

$$\ln\left[\gamma_l\left(\frac{1+\cos\theta}{2}\right)^2\right] = -2\beta\left(\gamma_s-\gamma_l\right)^2 + \ln\left(\gamma_s\right) \qquad (2)$$

The liquid surface energy is known and plotting the left side of (2) against γ_l will produce a parabolic curve of data points. A second-order polynomial regression of the plotted data allows for determination of the β parameter and γ_s.

3.2. Fowkes model

Fowkes surface energy theory combines the Young and Young-Dupree equation and dissociates liquid and solid surface energy into its polar and non-polar (dispersive) components [25]:

$$\frac{\gamma_l(cos\theta+1)}{2} = \left(\gamma_l^d\right)^{1/2}(\gamma_s^d)^{1/2} + \left(\gamma_l^p\right)^{1/2}\left(\gamma_s^p\right)^{1/2} \qquad (3)$$

where γ_l^d and γ_l^p are the liquid dispersive and polar components, respectively, and γ_s^d and γ_s^p are the solid dispersive and polar components, respectively. First, a nonpolar aprotic liquid, e.g., diiodomethane ($\gamma_l^p = 0$), is tested and the dispersive component of the solid surface energy, γ_s^d, is computed from (3). Second, a polar protic liquid, e.g., water, is tested and using γ_s^d and (3) the polar component of the solid surface energy, γ_s^p, is computed. Fowkes theory assumes that the total surface energy is the sum of the dispersive and polar components as shown in (4):

$$\gamma_s = \gamma_s^d + \gamma_s^p \qquad (4)$$

3.3. Owens-Wendt (extended Fowkes) model

Owens-Wendt theory (extended Fowkes) extends on the Fowkes model by incorporating Good's equation [9,17]:

$$\gamma_{sl} = \gamma_s + \gamma_l - 2\left(\gamma_s^d\gamma_l^d\right)^{1/2} - 2\left(\gamma_s^p\gamma_l^p\right)^{1/2} \qquad (5)$$

where γ_{sl} is the surface energy at the solid-liquid interface. Combining Young's equation with (5) yields:

$$\frac{\gamma_l(cos\theta + 1)}{2\left(\gamma_l^d\right)^{1/2}} = \left(\gamma_s^p\right)^{1/2}\frac{\left(\gamma_l^p\right)^{1/2}}{\left(\gamma_l^d\right)^{1/2}} + (\gamma_s^d)^{1/2} \quad (6)$$

The polar and dispersive components of the liquid surface energy are known and plotting the left side of equation 6 against $(\gamma_l^p)^{1/2}/(\gamma_l^d)^{1/2}$ will produce a linear line of data points. Linear regression of the data will allow for determination of γ_s^p as the square of the slope and γ_s^d as the square of the y-intercept.

4. Results

4.1. Sample Characterization

Figure 2 shows the Raman spectrum of G/Cu right after synthesis. The intensity of disorder-induced Raman D-peak at 1350 cm^{-1} is very low, indicating that the graphene film has very few defects. The peaks at 1595 and 2695 cm^{-1} are identified as G and 2D peaks, respectively, and their presence agrees well with previous G/Cu spectra [41,42]. The 2D peak shows a sharp single Lorentzian profile, which is a clear indication of monolayer graphene [41]. SEM and AFM data shows that the surface of G/Cu is rough due to the polycrystalline copper foil substrate (Figure S1 – S2). However, no apparent particulate contaminant was observed. In a previous study, G/Cu samples prepared using the same protocol as we used here showed a minimum graphene coverage of >99.9% on Cu foil [15].

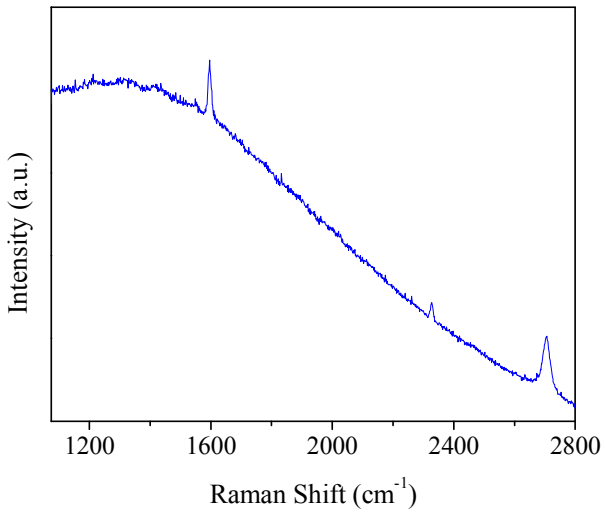

Figure 2. Raman spectrum of G/Cu. Note that the small peak at 2330 cm^{-1} is due to atmospheric N_2 [43].

4.2. Contact angle and surface energy

Contact angle data for the four test liquids is plotted in Figure 3 and average values are shown in Table 2. Figure 4 shows the polynomial fitting of data by Neumann's model and Figure 5 shows the linear fitting of data by Owens-Wendt (extended Fowkes) model. Table 3 lists the calculated total surface energy and β parameter for the Neumann model and the total surface energy and its polar and dispersive components for the Fowkes and Owens-Wendt models. As shown in Table 3, the surface energy of G/Cu is the highest immediately after synthesis and decreases with the exposure time in air. The surface energy of fresh G/Cu tested within 30 seconds of being removed from the CVD chamber was 52.99 mJ/m^2 (Owens-Wendt), 62.21 mJ/m^2 (Fowkes) and 63.84 mJ/m^2 (Neumann). The surface energy decreased after aging in ambient air for 1 hour and further decreased after 2 hours of aging. G/Cu exposed to ambient air for 24 hours showed the lowest surface energy of 37.54 mJ/m^2 (Owens-Wendt), 45.60 mJ/m^2 (Fowkes) and 57.44 mJ/m^2 (Neumann). According to the results from Owens-Wendt model, the polar component of surface energy, γ_s^p, is the greatest on fresh G/Cu and decreases by 75% after 24-hour exposure to air.

Meanwhile, the dispersive component, γ_s^d, decreases 13%. The results from Fowkes model show a similar trend, indicating that G/Cu surface is initially mildly polar and becomes increasingly non-polar upon exposure to air.

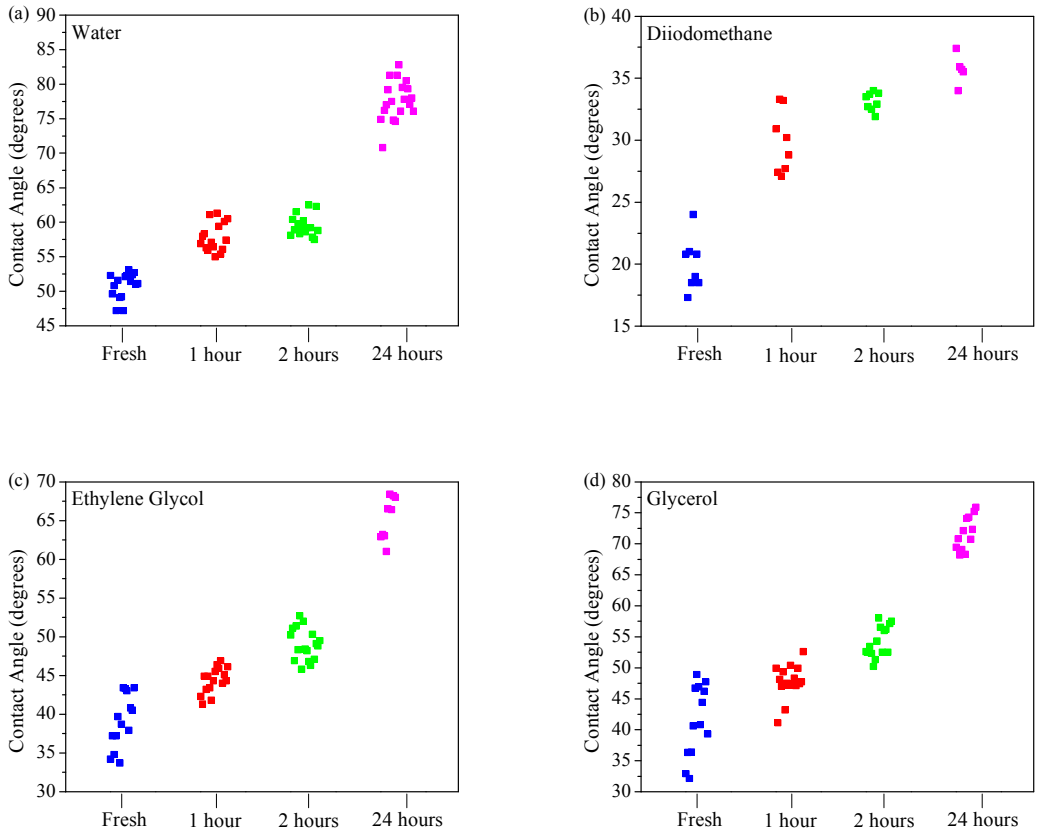

Figure 3. Contact angle data on G/Cu for (a) water, (b) diiodomethane, (c) ethylene glycol, and (d) glycerol. All data was taken at the time indicated on the x-axis and are shifted horizontally in the figures for clarity.

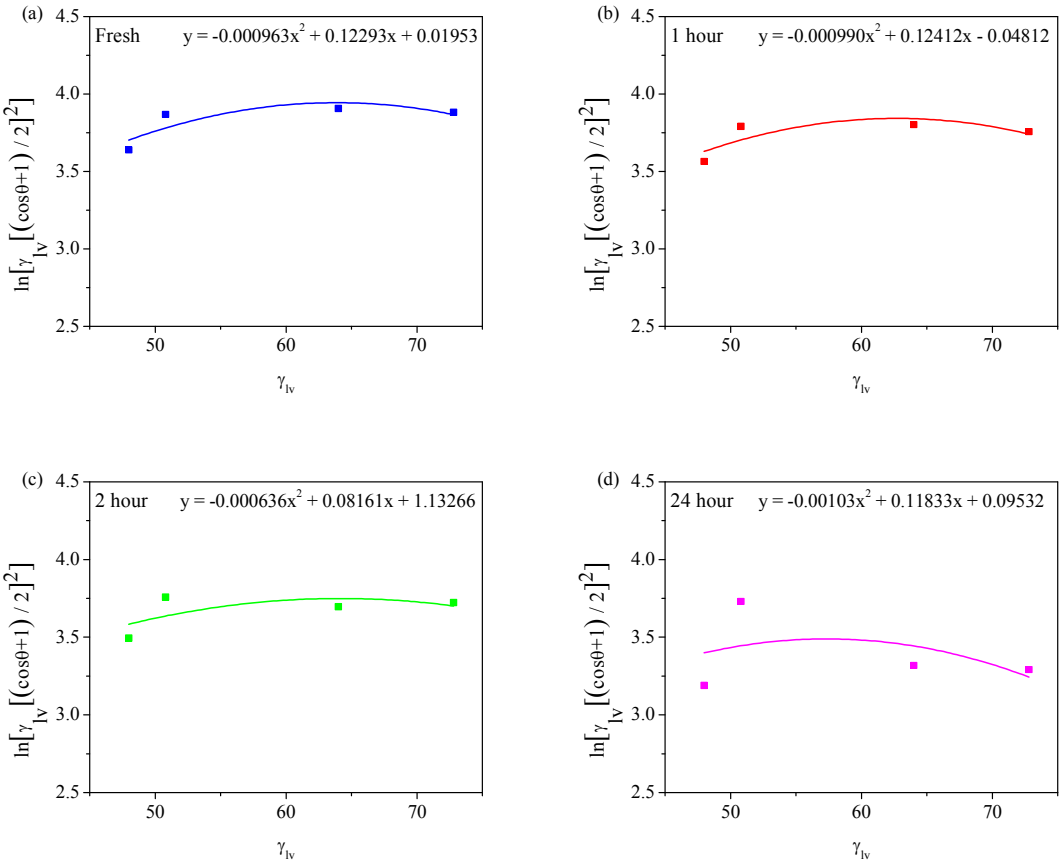

Figure 4. Neumann model plots for (a) fresh, (b) 1 hour aged, (c) 2 hour aged, and (d) 24 hour aged G/Cu.

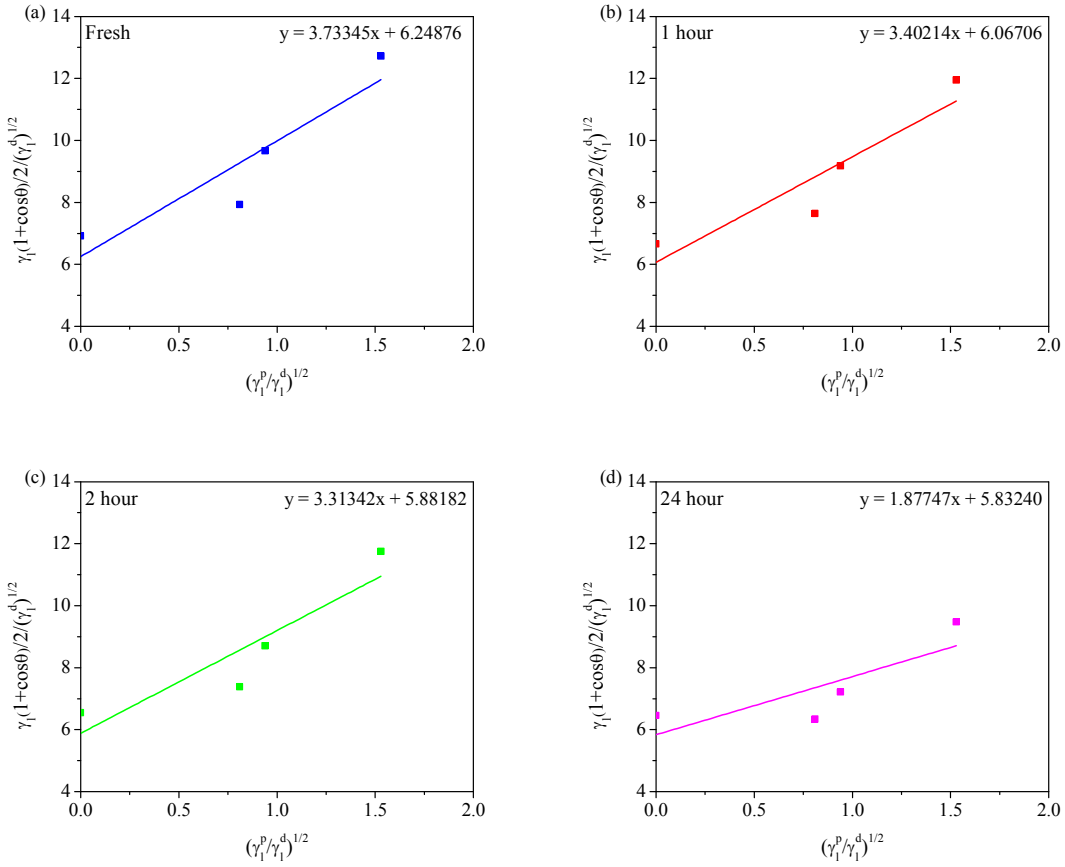

Figure 5. Owens-Wendt (extended Fowkes) plots for (a) fresh, (b) 1 hour aged, (c) 2 hour aged, and (d) 24 hour aged G/Cu.

Table 2. Contact angle data on G/Cu presented as average (standard deviation) of tests for water (W), diiodomethane (DIM), ethylene glycol (EG), and glycerol (G).

	W	DIM	EG	G
Fresh	50.82 (1.85)	19.99 (2.11)	38.75 (3.46)	40.39 (5.78)
1h air	57.83 (2.07)	29.83 (2.50)	44.39 (1.65)	47.76 (2.70)
2h air	59.52 (1.52)	33.13 (0.74)	48.95 (2.06)	54.19 (2.48)
24h air	77.55 (2.88)	35.70 (1.21)	65.01 (2.78)	71.70 (2.71)

Table 3. Surface free energy of G/Cu determined by Neumann, Fowkes, and Owens-Wendt models. Data presented as average (standard deviation).

G/Cu	Neumann model		Fowkes model			Owens-Wendt model		
	β	γ_s (mJ/m^2)	γ_s^p (mJ/m^2)	γ_s^d (mJ/m^2)	γ_s (mJ/m^2)	γ_s^p (mJ/m^2)	γ_s^d (mJ/m^2)	γ_s (mJ/m^2)
Fresh	0.00048138 (0.00023229)	**63.84 (1.97)**	14.42 (1.67)	47.79 (1.43)	**62.21 (3.10)**	13.94 (1.96)	39.05 (2.35)	**52.99 (4.31)**
1h aged	0.00049506 (0.00014586)	**62.68 (0.42)**	11.97 (1.70)	44.29 (1.82)	**56.27 (3.52)**	11.57 (1.82)	36.81 (1.69)	**48.38 (3.50)**
2h aged	0.00031820 (0.00004533)	**64.12 (0.47)**	11.57 (1.61)	42.88 (0.66)	**54.45 (2.27)**	10.98 (1.67)	34.60 (1.02)	**45.57 (2.69)**
24h aged	0.00051500 (0.00023892)	**57.44 (2.11)**	3.90 (2.75)	41.70 (1.13)	**45.60 (3.88)**	3.52 (2.53)	34.02 (0.23)	**37.54 (2.30)**

4.3. Ellipsometry

Figure 6 shows the evolution of phase shift on freshly-synthesized G/Cu surface as a function of air exposure time. The data was collected from the same spot on the G/Cu surface. All the x-values are shifted by 5 minutes to reflect transfer time of the sample from CVD chamber to ellipsometer stage. The increasing trend of phase shift shows clear evidence that a thin layer of adsorbate formed on G/Cu surface during the first two hours of air exposure. Interestingly, our previous work demonstrated a similar WCA increasing trend on fresh G/Cu surface due to airborne hydrocarbon contamination [15], further corroborating that the phase shift increase is induced by the adsorption of airborne hydrocarbons.

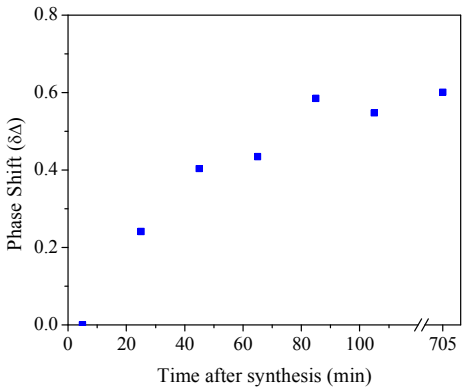

Figure 6. Phase shift (δΔ) on fresh G/Cu.

4.4 Effect of surface roughness

The Wenzel equation allows comparison of the experimentally determined apparent CA (θa) and the Young's CA (θ_Y) which is the contact angle determined on a smooth surface [44,45]:

$$\cos\theta_a = r\cos\theta_Y \qquad (7)$$

$$r = \frac{A_a}{A_p} \qquad (8)$$

where *r* is defined by the ratio of apparent surface area to projected surface area. The *r* value for

where *r* is defined by the ratio of apparent surface area to projected surface area. The *r* value for

our sample was determined by AFM to be in the range of 1.00095 to 1.0257 [45,46], depending on the scanning parameters (see the Supporting Document for details). Using the upper bound of the *r* value of 1.0257 and 50.86° measured WCA, the corresponding θ_Y value was found to be 51.98° for fresh G/Cu. The difference between θa and θ_Y in this case is only 1.1°. Noting that the uncertainty of WCA test is at least ±1°, we conclude that the error introduced by surface roughness is negligible on our G/Cu samples.

In addition to the above analysis, we also prepared monolayer graphene on ultra-flat Cu substrates (flat G/Cu, r = 1.00019) following a published procedure [47]. The WCA of fresh flat G/Cu was 56.33°±3.9° and increased to 81.15°±1.4° after 24 hours of air exposure. The WCA on flat G/Cu is about 5° greater than that on G/Cu foil. Unfortunately, because the two types of samples were prepared and measured in different buildings, it is likely that local air quality contributes to the difference in the WCA [48]; the 5° difference should be regarded as the upper limit of the roughness effect.

5. Discussion

5.1 Time dependence

The surface energy calculated by the Fowkes model matches the Neumann results very well on fresh graphene. The difference between the two models on fresh and 24 hour aged G/Cu is 3% and 21%, respectively. The Owens-Wendt model is an extension of the Fowkes approach and utilizes 4 liquids with different surface energies; therefore, the Owens-Wendt model is expected to be less dependent upon chosen test liquids. On fresh and 24 hour aged G/Cu, the difference between the Fowkes and Owens-Wendt models are 15% and 18%, respectively. The Neumann

approach is based on equation of state theory and introduces the surface dependent β parameter. Our calculations indicate that the Neumann surface energy is consistently higher than the Fowkes and Owens-Wendt models, although the Neumann and Fowkes results are similar on fresh G/Cu. It has been proposed that β = 0.0001247 can be expressed as a universal constant that is independent of test solid [22]. Neumann model fitting of our data indicates that β of G/Cu is ~4 times greater than the proposed universal constant and increases ~7% from fresh to aged surface. Regardless of the model used to determine the surface energy values, the surface energy of G/Cu always decreased with air exposure time. This decrease can be attributed to the hydrocarbon contamination. Recently, Gomez-Herrero *et al.* reported aromatic hydrocarbon contamination on graphite by Kelvin probe force microscopy and suggested that the contaminants desorb near 50°C [16]. Additionally, Li *et al.* reported contamination of graphene surfaces by airborne hydrocarbons [15]. Once freshly synthesized G/Cu was exposed to ambient air, hydrocarbons would adsorb onto the initially high-energy surface and WCA would concurrently decrease. They substantiated the hydrocarbon contamination theory with ATR-FTIR and XPS experiments showing that hydrocarbon species were initially absent and appeared after exposure to air for a period of time [15]. Moreover, recent theoretical work has suggested that graphitic surfaces are intrinsically hydrophilic [49,50]. In the current paper, spectroscopic ellipsometry results on fresh G/Cu further support this conclusion. As shown in Figure 6, the phase shift change (δΔ) of fresh G/Cu sample increases with the air exposure time, indicating adsorption of airborne hydrocarbon contaminants [32,33]. As a result, the surface energy of the fresh G/Cu sample is the highest. To lower the surface energy, G/Cu adsorbs airborne hydrocarbon as shown by ellipsometry results.

The change in WCA can be related to the extent of hydrocarbon contamination as shown in Figure 7. The ellipsometric phase shift (Figure 6) indicates hydrocarbon contamination of fresh G/Cu and its inverse linear relationship with cos(θ) of the WCA provides a correlation between

extent of contamination and WCA measurement. The linearity corroborates a Cassie-Baxter relationship [9,51], though the ellipsometry and WCA experiments were conducted in different labs, suggesting that a simple WCA measurement on G/Cu can indicate the degree of surface contamination.

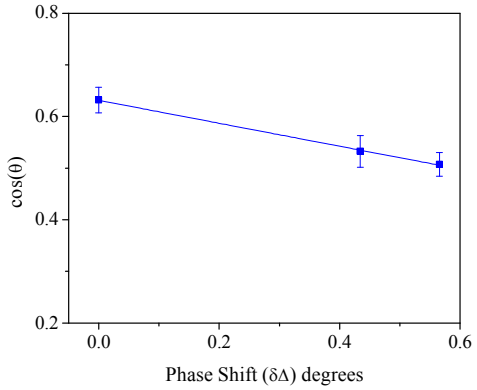

Figure 7. Correlation between WCA (θ) and ellipsometry phase shift on fresh, 1h aged, and 2h aged G/Cu. Accuracy of the phase shift (Δ) is 0.1% [52]. The solid line is a linear fit of the data: $y=-0.222*x+0.631$ and $r^2=0.99$.

The surface energy of graphene reported by Coleman [20] is 65-90 mJ/m^2, slightly higher than our results. However, since very different material system, experimental method and theoretical model was involved in their work, direct comparison is difficult. In contrast, it makes more sense to compare our results to Wang's [7] since they also determined the surface energy by contact angle testing and using Newmann model. Wang reported 46.7 mJ/m^2 for the surface energy of graphene, which is significantly lower than 63.8 mJ/m^2 as we found for the fresh G/Cu. There are three possible reasons for the difference. First, the hydrocarbon contamination was not considered at all in Wang's work and it is not clear how that will affect the surface energy value. Second, our graphene sample is single-layer CVD graphene on copper while Wang's graphene is a "thick" film synthesized by the reduction of graphene oxide. As a result, the chemistry of the two

graphene samples may not be exactly the same. Third, Wang's analysis included a fifth test liquid, formamide, which will likely affect the model results.

5.2 Intrinsic polarity

According to the results from both Fowkes model and Owen-Wendt model, the polar component of the total surface energy of fresh G/Cu is significant; indicating G/Cu intrinsically has a mildly polar (hydrophilic) surface. However, since it is generally accepted that, at atomic level, graphene has non-polar sp^2 structure, why is G/Cu surface mildly polar? We suggest that the mild polarity of G/Cu can be attributed to three factors: π hydrogen bonding, surface defects, and partial wetting transparency.

First, a few recent theoretical studies showed that the binding energy of water molecule on graphite is higher than previously reported values, mostly in the range of −10 kJ/mol to −13 kJ/mol [53–55]. Interestingly, these studies also concluded that the preferred orientation of adsorbed water molecule is with the hydrogen pointing to graphene, suggesting the presence of a H···π interaction [53–55], also known as π hydrogen bonding. Such interaction has been previously observed for water interacting with small conjugated molecules, such as benzene, and could be significantly enhanced by the extended π system of graphene [53,56]. Although more study is required to fully understand this effect, the π hydrogen bonding could contribute to the observed intrinsic polarity of G/Cu. Second, the existence of the defects on graphene/graphite surface could also contribute to its intrinsic polarity, as is evidenced both theoretically [57] and experimentally [10,58]. Also, such defect sites on graphene/graphite surface have been implicated as nucleation sites for adsorption of organic molecules due to their high surface energy [59]. This hypothesis is supported by an increase of surface inhomogeneity indicated by increasing contact angle hysteresis upon exposure to air [15,42]. It is not clear at this point if these defects are chemical or topographical in nature. However, regardless of the exact nature, these defects with high surface

energy could contribute to the observed polarity of G/Cu. Third, the copper substrate could contribute to the polarity as well. Since graphene is only one atom thick, the underlying substrate could interact with the liquid droplet on top of the graphene and contribute to the surface energy of G/Cu. Indeed, several recent reports did show that graphene is (at least partially) transparent regarding the interaction between water and the underlying substrate [4,15,60]. Shih *et al.* showed partial wetting transparency on graphene through molecular dynamics (MD) simulations [60] and Li's WCA results supported the conclusion [15]. Since copper is very hydrophilic [55], it can make the G/Cu surface more polar via partial transparency effect.

This transparency effect can be further elucidated by comparing the surface energy of G/Cu to that of HOPG, which can be considered as infinite layers of graphene. Surface energies calculated (Table S1 and S2) by Neumann, Fowkes, and Owens-Wendt models indicate that fresh HOPG surface exhibits surface energy of 60.23 mJ/m^2, 55.40 mJ/m^2, and 51.60 mJ/m^2, respectively. For both the Neumann and Owens-Wendt models, the surface energy of G/Cu is higher than HOPG. Moreover, according to Fowkes and Owens-Wendt models, the polar surface energy of G/Cu is higher than that of HOPG. This observation is consistent with partial-wetting transparency theory although we cannot exclude the possibility that the intrinsic defects of G/Cu and HOPG are slightly different and could play a role. Moreover, WCA data reported by Li *et al.* on G/Cu, G/Nickel, and HOPG supports the partial-wetting transparency effect which suggests that the substrate may contribute to the polarity of G/Cu [15].

Finally, it was recently reported that oxygen can intercalate between graphene and copper upon ambient air exposure [61,62]. Depending on the charge state of the oxygen, the intercalation could potentially increase the polarity of the G/Cu surface and contribute to the observed time evolution of the WCA. Additional studies are needed to separate the effect of hydrocarbon contamination and oxygen intercalation on the wettability of supported graphene.

6. Conclusion

Our study showed that the WCA of fresh G/Cu is 51° and its surface energy was 62.2 mJ/m^2 (Fowkes), 53.0 mJ/m^2 (Owens-Wendt) and 63.8 mJ/m^2 (Neumann). Aging in air for 1-2 hours consequently increases contact angle and concurrently decreases surface energy. The initially high-energy graphene attracts airborne hydrocarbons, which subsequently are adsorbed on the graphene surface and "shield" the polar surface sites and thus decrease the overall surface energy. The WCA of 24 hour aged G/Cu was 78° and its surface energy was 45.6 mJ/m^2 (Fowkes), 37.5 mJ/m^2 (Owens-Wendt) and 57.4 mJ/m^2 (Neumann). The intrinsic mild polarity of G/Cu was explained in terms of high energy surface defects, π-hydrogen bonding, and partial wetting transparency.

Acknowledgement

L. L. and H. L. thank Taiho Kogyo Tribology Research Foundation for financial support.

References

(1) Geim, A. K.; Novoselov, K. S. The Rise of Graphene. *Nat. Mater.* **2007**, *6*, 183–191.

(2) Zhu, Y.; Murali, S.; Cai, W.; Li, X.; Suk, J. W.; Potts, J. R.; Ruoff, R. S. Graphene and Graphene Oxide: Synthesis, Properties, and Applications. *Adv. Mater.* **2010**, *22*, 3906–3924.

(3) Lee, C.; Li, Q.; Kalb, W.; Liu, X.-Z.; Berger, H.; Carpick, R. W.; Hone, J. Frictional Characteristics of Atomically Thin Sheets. *Science* **2010**, *328*, 76–80.

(4) Rafiee, J.; Mi, X.; Gullapalli, H.; Thomas, A. V; Yavari, F.; Shi, Y.; Ajayan, P. M.; Koratkar, N. a. Wetting Transparency of Graphene. *Nat. Mater.* **2012**, *11*, 217–222.

(5) Zhu, Y.; Murali, S.; Stoller, M. D.; Ganesh, K. J.; Cai, W.; Ferreira, P. J.; Pirkle, A.; Wallace, R. M.; Cychosz, K. A.; Thommes, M.; et al. Carbon-Based Supercapacitors Produced by Activation of Graphene. *Science* **2011**, *332*, 1537–1541.

(6) Ghosh, S.; An, X.; Shah, R.; Rawat, D.; Dave, B.; Kar, S.; Talapatra, S. Effect of 1-Pyrene Carboxylic-Acid Functionalization of Graphene on Its Capacitive Energy Storage. *J. Phys. Chem. C* **2012**, *116*, 20688–20693.

(7) Wang, S.; Zhang, Y.; Abidi, N.; Cabrales, L. Wettability and Surface Free Energy of Graphene Films. *Langmuir* **2009**, *25*, 11078–11081.

(8) Koenig, S. P.; Boddeti, N. G.; Dunn, M. L.; Bunch, J. S. Ultrastrong Adhesion of Graphene Membranes. *Nat. Nanotechnol.* **2011**, *6*, 543–546.

(9) Selvakumar, N.; Barshilia, H. C.; Rajam, K. S. Effect of Substrate Roughness on the Apparent Surface Free Energy of Sputter Deposited Superhydrophobic Polytetrafluoroethylene Coatings: A Comparison of Experimental Data with Different Theoretical Models. *J. Appl. Phys.* **2010**, *108*, 013505.

(10) Shin, Y. J.; Wang, Y.; Huang, H.; Kalon, G.; Wee, A. T. S.; Shen, Z.; Bhatia, C. S.; Yang, H. Surface-Energy Engineering of Graphene. *Langmuir* **2010**, *26*, 3798–3802.

(11) Schedin, F.; Geim, A.; Morozov, S. V; Hill, E. W.; Blake, P.; Katsnelson, M. I.; Novoselov, K. S. Detection of Individual Gas Molecules Adsorbed on Graphene. *Nat. Mater.* **2007**, *6*, 652–655.

(12) Kim, K.-S.; Lee, H.-J.; Lee, C.; Lee, S.-K.; Jang, H.; Ahn, J.-H.; Kim, J.-H.; Lee, H.-J. Chemical Vapor Deposition-Grown Graphene: The Thinnest Solid Lubricant. *ACS Nano* **2011**, *5*, 5107–5114.

(13) Adamson, A. W.; Gast, A. P. *Physical Chemistry of Surfaces*; 6th ed.; John Wiley & Sons, Inc.: New York, 1997.

(14) Fowkes, F.; Harkins, D. The State of Monolayers Adsorbed at the Interface Solid-Aqueous Solution. *J. Am. Chem. Soc.* **1940**, *62*, 3377.

(15) Li, Z.; Wang, Y.; Kozbial, A.; Shenoy, G.; Zhou, F.; McGinley, R.; Ireland, P.; Morganstein, B.; Kunkel, A.; Surwade, S. P.; et al. Effect of Airborne Contaminants on the Wettability of Supported Graphene and Graphite. *Nat. Mater.* **2013**, *12*, 925–931.

(16) Martinez-Martin, D.; Longuinhos, R.; Izquierdo, J. G.; Marele, A.; Alexandre, S. S.; Jaafar, M.; Gómez-Rodríguez, J. M.; Bañares, L.; Soler, J. M.; Gomez-Herrero, J. Atmospheric Contaminants on Graphitic Surfaces. *Carbon* **2013**, *61*, 33–39.

(17) Owens, D. K.; Wendt, R. C. Estimation of the Surface Free Energy of Polymers. *J. Appl. Polym. Sci.* **1969**, *13*, 1741–1747.

(18) Li, D.; Neumann, A. W. Contact Angles on Hydrophobic Solid Surfaces and Their Interpretation. *J. Colloid Interface Sci.* **1992**, *148*, 190–200.

(19) Zhu, H.; Qin, X.; Sun, X.; Yan, W.; Yang, J.; Xie, Y. Rocking-Chair Configuration in Ultrathin Lithium Vanadate-Graphene Hybrid Nanosheets for Electrical Modulation. *Sci. Rep.* **2013**, *3*, 1246.

(20) Hernandez, Y.; Nicolosi, V.; Lotya, M.; Blighe, F. M.; Sun, Z.; De, S.; McGovern, I. T.; Holland, B.; Byrne, M.; Gun'Ko, Y. K.; et al. High-Yield Production of Graphene by Liquid-Phase Exfoliation of Graphite. *Nat. Nanotechnol.* **2008**, *3*, 563–568.

(21) Wang, Q.; Kalantar-Zadeh, K.; Kis, A. Electronics and Optoelectronics of Two-Dimensional Transition Metal Dichalcogenides. *Nature* **2012**, *7*, 699–712.

(22) Deshmukh, R. R.; Shetty, A. R. Comparison of Surface Energies Using Various Approaches and Their Suitability. *J. Appl. Polym. Sci.* **2008**, *107*, 3707–3717.

(23) Kwok, D. Y.; Ng, H.; Neumann, A. W. Experimental Study on Contact Angle Patterns: Liquid Surface Tensions Less Than Solid Surface Tensions. *J. Colloid Interface Sci.* **2000**, *225*, 323–328.

(24) Dalal, E. N. Calculation of Solid Surface Tensions. *Langmuir* **1987**, *3*, 1009–1015.

(25) Fowkes, F. M. Additivity of Intermolecular Forces at Interfaces. I. Determination of the Contribution to Surface and Interfacial Tensions of Dispersion Forces in Various Liquids. *J. Phys. Chem.* **1963**, *67*, 2538–2541.

(26) Subedi, D. P. Contact Angle Measurement for the Surface Characterization of Solids. *Himal. Phys.* **2011**, *11*, 1–4.

(27) Surwade, S. P.; Li, Z.; Liu, H. Thermal Oxidation and Unwrinkling of Chemical Vapor Deposition-Grown Graphene. *J. Phys. Chem. C* **2012**, *116*, 20600–20606.

(28) Zhao, S.; Surwade, S. P.; Li, Z.; Liu, H. Photochemical Oxidation of CVD-Grown Single Layer Graphene. *Nanotechnology* **2012**, *23*, 355703.

(29) Roche, A.; Wyon, C.; Marthon, S.; Ple, J. F.; Olivier, M.; Rochat, N.; Chabli, A.; Danel, A.; Juhel, M.; Tardif, F. Detection of Organic Contamination on Silicon Substrates : Comparison of Several Techniques. *AIP Conf. Proc.* **2001**, *550*, 297–301.

(30) Koster, G.; Rijnders, G. *In Situ Characterization of Thin Film Growth*; Woodhead Publishing: Cambridge, 2011.

(31) Nham, H. S.; Hess, G. B. Ellipsometric Study of Krypton, Methane, and Argon Films on Graphite: How Complete Is Wetting? *Langmuir* **1989**, *5*, 575–582.

(32) Fukuzawa, K.; Shimuta, T.; Nakada, A.; Zhang, H.; Mitsuya, Y. Measurement of Thickness of Molecularly Thin Lubricant Film Using Ellipsometric Microscopy. *IEEE Trans. Magn.* **2005**, *41*, 808–811.

(33) McMillan, T.; Rutledge, J. E.; Taborek, P. Ellipsometry of Liquid Helium Films on Gold, Cesium, and Graphite. *J. Low Temp. Phys.* **2005**, *138*, 995–1011.

(34) Prunici, P.; Hess, P. Ellipsometric in Situ Measurement of Oxidation Kinetics and Thickness of (C2–C20) Alkylsilyl (sub)monolayers. *J. Appl. Phys.* **2008**, *103*, 024312.

(35) Kloubek, J. A. N. Development of Methods for Surface Free Energy Determination Using Contact Angles of Liquids on Solids. *Adv. Colloid Interface Sci.* **1992**, *38*, 99–142.

(36) Sharma, P. K.; Rao, K. H. Analysis of Different Approaches for Evaluation of Surface Energy of Microbial Cells by Contact Angle Goniometry. *Adv. Colloid Interface Sci.* **2002**, *98*, 341–463.

(37) Chibowski, E.; Perea-Carpio, R. Problems of Contact Angle and Solid Surface Free Energy Determination. *Adv. Colloid Interface Sci.* **2002**, *98*, 245–264.

(38) Good, R. J. Contact Angle, Wetting, and Adhesion: A Critical Review. *J. Adhes. Sci. Technol.* **1992**, *6*, 1269–1302.

(39) Li, D.; Neumann, A. W. Equilibrium of Capillary Systems with an Elastic Liquid-Vapor Interface. *Langmuir* **1993**, *9*, 50–54.

(40) Neumann, A. W.; Good, R. J.; Hope, C. J.; Sejpal, M. An Equation-of-State Approach to Determine Surface Tensions of Low-Energy Solids from Contact Angles. *J. Colloid Interface Sci.* **1974**, *49*, 291–304.

(41) Ferrari, A. C.; Meyer, J. C.; Scardaci, V.; Casiraghi, C.; Lazzeri, M.; Mauri, F.; Piscanec, S.; Jiang, D.; Novoselov, K. S.; Roth, S.; et al. Raman Spectrum of Graphene and Graphene Layers. *Phys. Rev. Lett.* **2006**, *97*, 187401.

(42) Reina, A.; Jia, X.; Ho, J.; Nezich, D.; Son, H.; Bulovic, V.; Dresselhaus, M. S.; Kong, J. Large Area, Few-Layer Graphene Films on Arbitrary Substrates by Chemical Vapor Deposition. *Nano Lett.* **2009**, *9*, 30–35.

(43) Hyatt, H. A.; Cherlow, J. M.; Fenner, W. R.; Porto, S. P. S. Cross Section for the Raman Effect in Molecular Nitrogen Gas. *J. Opt. Soc. Am.* **1973**, *63*, 1604–1606.

(44) Wenzel, R. Resistance of Solid Surfaces to Wetting by Water. *Ind. Eng. Chem.* **1936**, *28*, 988–994.

(45) Ramón-Torregrosa, P. J.; Rodríguez-Valverde, M. A.; Amirfazli, A.; Cabrerizo-Vílchez, M. A. Factors Affecting the Measurement of Roughness Factor of Surfaces and Its Implications for Wetting Studies. *Colloids Surfaces A Physicochem. Eng. Asp.* **2008**, *323*, 83–93.

(46) Poon, C. Y.; Bhushan, B. Comparison of Surface Roughness Measurements by Stylus Profiler, AFM and Non-Contact Optical Profiler. *Wear* **1995**, *190*, 76–88.

(47) Dhingra, S.; Hsu, J.-F.; Vlassiouk, I.; D'Urso, B. Chemical Vapor Deposition of Graphene on Large-Domain Ultra-Flat Copper. *Carbon* **2013**, *69*, 188–193.

(48) Not so Transparent. *Nat. Mater.* **2013**, *12*, 865.

(49) Sharma, M.; Donadio, D.; Schwegler, E.; Galli, G. Probing Properties of Water under Confinement: Infrared Spectra. *Nano Lett.* **2008**, *8*, 2959–2962.

(50) Wu, Y.; Aluru, N. R. Graphitic Carbon-Water Nonbonded Interaction Parameters. *J. Phys. Chem. B* **2013**, *117*, 8802–8813.

(51) Cassie, A. B. D.; Baxter, S. Wettability of Porous Surfaces. *Trans. Faraday Soc.* **1944**, *40*, 546–551.

(52) Johs, B.; Herzinger, C. M. Quantifying the Accuracy of Ellipsometer Systems. *Phys. Status Solidi* **2008**, *5*, 1031–1035.

(53) Hamada, I. Adsorption of Water on Graphene: A van Der Waals Density Functional Study. *Phys. Rev. B* **2012**, *86*, 195436.

(54) Voloshina, E.; Usvyat, D.; Schütz, M.; Dedkov, Y.; Paulus, B. On the Physisorption of Water on Graphene: A CCSD(T) Study. *Phys. Chem. Chem. Phys.* **2011**, *13*, 12041–12047.

(55) Rubes, M.; Kysilka, J.; Nachtigall, P.; Bludský, O. DFT/CC Investigation of Physical Adsorption on a Graphite (0001) Surface. *Phys. Chem. Chem. Phys.* **2010**, *12*, 6438–6444.

(56) Suzuki, S.; Green, P. G.; Bumgarner, R. E.; Dasgupta, S.; Goddard, W. A.; Blake, G. A. Benzene Forms Hydrogen Bonds with Water. *Science* **1992**, *257*, 942–945.

(57) Ghaderi, N.; Peressi, M. First-Principle Study of Hydroxyl Functional Groups on Pristine, Defected Graphene, and Graphene Epoxide. *J. Phys. Chem. C* **2010**, *114*, 21625–21630.

(58) Zhou, H.; Ganesh, P.; Presser, V.; Wander, M. C. F.; Fenter, P.; Kent, P. R. C.; Jiang, D.; Chialvo, A. a.; McDonough, J.; Shuford, K. L.; et al. Understanding Controls on Interfacial Wetting at Epitaxial Graphene: Experiment and Theory. *Phys. Rev. B* **2012**, *85*, 035406.

(59) Xu, K.; Heath, J. R. Contact with What? *Nat. Mater.* **2013**, *12*, 12–13.

(60) Shih, C.-J.; Wang, Q. H.; Lin, S.; Park, K.-C.; Jin, Z.; Strano, M. S.; Blankschtein, D. Breakdown in the Wetting Transparency of Graphene. *Phys. Rev. Lett.* **2012**, *109*, 176101.

(61) Kidambi, P. R.; Bayer, B. C.; Blume, R.; Wang, Z.-J.; Baehtz, C.; Weatherup, R. S.; Willinger, M.-G.; Schloegl, R.; Hofmann, S. Observing Graphene Grow: Catalyst-Graphene Interactions during Scalable Graphene Growth on Polycrystalline Copper. *Nano Lett.* **2013**, *13*, 4769–4778.

(62) Kimouche, A.; Renault, O.; Samaddar, S.; Winkelmann, C.; Fruchart, O.; Coraux, J. Modulating Charge Density and Inelastic Optical Response in Graphene by

Atmospheric Pressure Localized Intercalation through Wrinkles. *Carbon* **2014**, *68*, 73–79.

TOC Figure

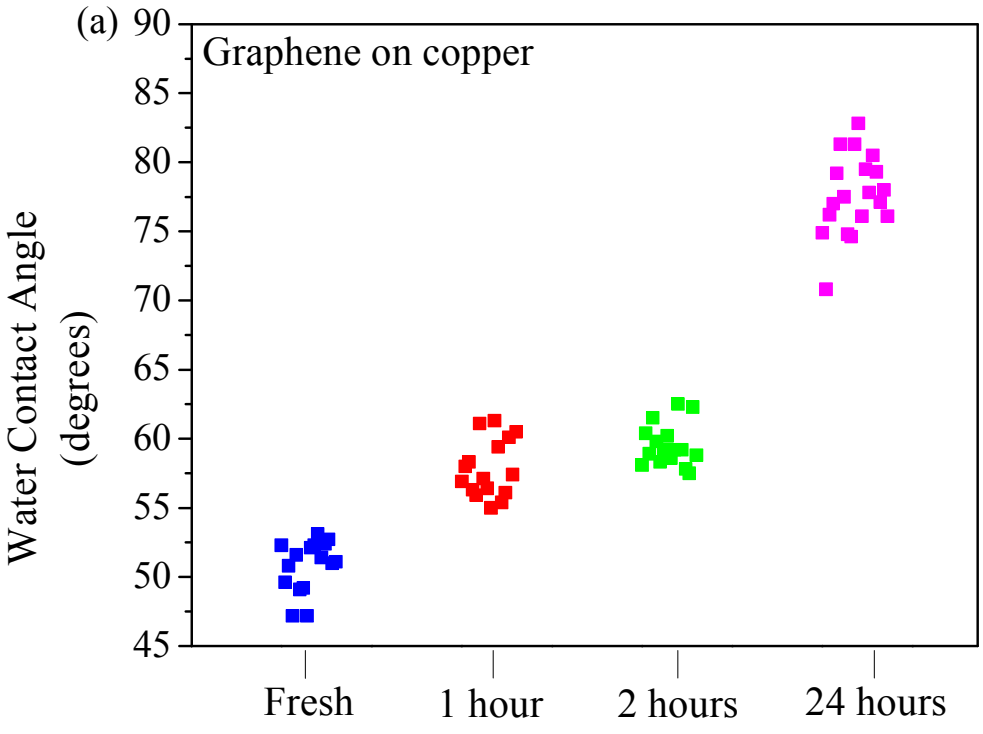
(a)
Graphene on copper
Water Contact Angle (degrees)
90
85
80
75
70
65
60
55
50
45
Fresh
1 hour
2 hours
24 hours